Arch Appl Mech (2010) 80: 1163–1175
DOI 10.1007/s00419-010-0430-y

ORIGINAL

Sergio A. Oliveira · Marcelo A. Savi · Alexander L. Kalamkarov

A three-dimensional constitutive model for shape memory alloys

Received: 21 May 2009 / Accepted: 6 April 2010 / Published online: 24 April 2010

Abstract Shape memory alloys (SMAs) are materials that, among other characteristics, have the ability to present high deformation levels when subjected to mechanical loading, returning to their original form after a temperature change. Literature presents numerous constitutive models that describe the phenomenological features of the thermomechanical behavior of SMAs. The present paper introduces a novel three-dimensional constitutive model that describes the martensitic phase transformations within the scope of standard generalized materials. The model is capable of describing the main features of the thermomechanical behavior of SMAs by considering four macroscopic phases associated with austenitic phase and three variants of martensite. A numerical procedure is proposed to deal with the nonlinearities of the model. Numerical simulations are carried out dealing with uniaxial and multiaxial single-point tests showing the capability of the introduced model to describe the general behavior of SMAs. Specifically, uniaxial tests show pseudoelasticity, shape memory effect, phase transformation due to temperature change and internal subloops due to incomplete phase transformations. Concerning multiaxial tests, the pure shear stress and hydrostatic tests are discussed showing qualitatively coherent results. Moreover, other tensile–shear tests are conducted modeling the general three-dimensional behavior of SMAs. It is shown that the multiaxial results are qualitative coherent with the related data presented in the literature.

Keywords Shape memory alloys · Constitutive model · Pseudoelasticity

1 Introduction

Shape memory alloys (SMAs) belong to the class of smart materials being used in different kinds of applications, see e.g. [10,14,21] and [9]. The remarkable properties of SMAs are associated with thermoelastic martensitic transformations that are responsible for different kinds of complex thermomechanical behavior of these smart materials. Besides pseudoelastic and shape memory effects, SMAs may demonstrate interesting behavior as internal subloops due to incomplete phase transformations, two-way shape memory effect, plasticity, transformation-induced plasticity, rate-dependency, thermomechanical couplings among other interesting effects related to nonhomogeneous characteristics. All these phenomena give a general idea about the complex thermomechanical behavior of SMAs, as discussed by [6,11,16,20,24,31] and [10].

S. A. Oliveira · M. A. Savi (✉)
COPPE—Department of Mechanical Engineering, Universidade Federal do Rio de Janeiro, P.O. Box 68.503, Rio de Janeiro, RJ 21.941.972, Brazil
E-mail: savi@mecanica.ufrj.br

A. L. Kalamkarov
Department of Mechanical Engineering, Dalhousie University, Halifax, Nova Scotia, Canada
E-mail: alex.kalamkarov@dal.ca

The modeling and simulation of thermomechanical behavior of SMAs is the objective of numerous research efforts. SMA can be modeled on the microscopic, mesoscopic or macroscopic levels. The macroscopic modeling is related to phenomenological features, and it relies on the continuum thermodynamics with internal state variables to take into account the changes in the microstructure due to phase transformation [21,25]. Paiva & Savi [21] and Lagoudas [10] have presented a general overview of the SMA modeling, with the emphasis on the phenomenological constitutive models.

The SMA modeling becomes even more complex when three-dimensional media is of concern. Although many constitutive models are developed for a three-dimensional description, their verification is difficult due to the lack of experimental data. Therefore, many articles in literature present three-dimensional models but only discuss results related to the uniaxial tests. Nevertheless, some research efforts are dedicated to show results related to the multiaxial tests and, among others, one could refer to some of them: [2,4,5,13,23,25,32,34].

Besides the thermomechanical modeling of SMAs, some experimental reports are of a great importance in order to validate the three-dimensional models. Among other efforts, one could refer to some experimental multiaxial tests performed in different contexts: [7,15,17,27].

In this regard, the present work proposes a three-dimensional constitutive model developed within the framework of continuum mechanics and generalized standard materials being built upon the classical Fremond's model [5]. The model is inspired on the one-dimensional model that is able to describe different thermomechanical behaviors of SMAs in a flexible way, and its numerical simulations are in a close agreement with the experimental uniaxial tests [3,18,22,28,29]. Numerical simulations are carried out for both uniaxial and multiaxial tests considering a single-point analysis that shows that the introduced model is able to capture the general thermomechanical behavior of SMAs.

2 Constitutive equations

Modeling of SMA behavior can be done within the scope of standard generalized materials under the assumption that the thermodynamic state of the material can be completely defined by a finite number of state variables, see e.g. [12]. Under this assumption, the thermomechanical behavior can be described by the Helmholtz free energy density, Ψ, and the pseudo-potential of dissipation, Φ.

Experimental studies have revealed the main aspects of the thermomechanical behavior of SMAs. Basically, there are two possible phases: austenite and martensite. In martensitic phase, different deformation orientations of crystallographic plates constitute what is known by the martensitic variants. In the case of three-dimensional medium, there are 24 possible martensitic variants that are arranged in 6 plate groups with 4 plate variants per group. Because the crystal structure of martensite is less symmetric than the austenite, only a single variant is created on the reverse transformation [30,35].

The three-dimensional description of thermomechanical behavior of SMAs is usually inspired on one-dimensional models employing a limited number of martensitic variants. Motivated by one-dimensional models, the proposed model considers four macroscopic phases: austenite (A), the twinned martensite (M), which is stable in the absence of a stress field, and two other martensitic phases ($M+$ and $M-$). The definition of the Helmholtz free energy density considers different expressions for each one of the macroscopic phases, assuming that they are functions of strain, ε_{ij}, and temperature, T.

$$\begin{aligned}
M+ &: \rho\Psi_1(\varepsilon_{ij},T) = \frac{1}{2}\left(\lambda^M\varepsilon_{kk}^2 + 2\mu^M\varepsilon_{ij}\varepsilon_{ij}\right) - \alpha\Gamma - \Lambda_M - \Omega_{ij}^M(T-T_0)\varepsilon_{ij}\\
M- &: \rho\Psi_2(\varepsilon_{ij},T) = \frac{1}{2}\left(\lambda^M\varepsilon_{kk}^2 + 2\mu^M\varepsilon_{ij}\varepsilon_{ij}\right) + \alpha\Gamma - \Lambda_M - \Omega_{ij}^M(T-T_0)\varepsilon_{ij}\\
A &: \rho\Psi_3(\varepsilon_{ij},T) = \frac{1}{2}\left(\lambda^A\varepsilon_{kk}^2 + 2\mu^A\varepsilon_{ij}\varepsilon_{ij}\right) - \Lambda_A - \Omega_{ij}^A(T-T_0)\varepsilon_{ij}\\
M &: \rho\Psi_4(\varepsilon_{ij},T) = \frac{1}{2}\left(\lambda^M\varepsilon_{kk}^2 + 2\mu^M\varepsilon_{ij}\varepsilon_{ij}\right) + \Lambda_M - \Omega_{ij}^M(T-T_0)\varepsilon_{ij}
\end{aligned} \tag{1}$$

Here, the indices M and A are related to the martensitic and austenitic phases, respectively; λ and μ are the Lamé coefficients; α is a scalar parameter related to the hysteresis loop; In Eq. (1), Λ_M and Λ_A are temperature functions that define the stress level of phase transformation; Ω_{ij} is a tensor related to the thermal expansion coefficients; T_0 is a reference temperature where stress-free state is free of strain; finally, ρ is the material

density. Moreover,

$$\Gamma = \frac{1}{3}(\varepsilon_{kk}) + \frac{2}{3}\sqrt{3}\left|\sqrt{J_2}\right| \operatorname{sign}(\varepsilon_{kk}) \tag{2}$$

where J_2 is a measurement of equivalent strain given by:

$$J_2 = \frac{1}{6}\left[(\varepsilon_{11}-\varepsilon_{22})^2 + (\varepsilon_{11}-\varepsilon_{33})^2 + (\varepsilon_{22}-\varepsilon_{33})^2 + 3\left(\varepsilon_{12}^2+\varepsilon_{21}^2+\varepsilon_{13}^2+\varepsilon_{31}^2+\varepsilon_{23}^2+\varepsilon_{32}^2\right)\right] \tag{3}$$

$\varepsilon_{kk} = \varepsilon_{11} + \varepsilon_{22} + \varepsilon_{33}$ and $\operatorname{sign}(\varepsilon_{kk})$ is defined as follows:

$$\operatorname{sign}(\varepsilon_{kk}) = \begin{cases} +1 & \text{if } \varepsilon_{kk} \geq 0 \\ -1 & \text{if } \varepsilon_{kk} < 0 \end{cases} \tag{4}$$

The variable Γ can be understood as an equivalent strain field that contributes to phase transformations. Its definition takes into account that phase transformations may be induced either by volumetric expansion (represented by the first term, $\varepsilon_{kk}/3$) or by deviatoric effect (represented by the second term, $(2\sqrt{3}/3)\left|\sqrt{J_2}\right| \operatorname{sign}(\varepsilon_{kk})$). This hypothesis is based on experimental observations that show that both effects induce phase transformation. It is important to highlight experimental torsion tests that indicate that stress–strain curves are qualitatively similar to those obtained in tensile tests [1,8,15]. Under this assumption, the equivalent field Γ may be interpreted as a phase transformation inductor that defines what kind of martensitic variant is induced. On the one hand, if $\Gamma \geq 0$, the variant $M+$ is induced. On the other hand, the variant M− is induced when $\Gamma < 0$. Note that each variant can be induced either by volumetric or by shear effects, allowing a proper description of the three-dimensional behavior. Moreover, it should be pointed out that, since the sign of shear strains does not appear in this inductor, they have a neutral influence, tending to follow the volumetric expansion influence. Besides, note that for one-dimensional case, $\Gamma = \varepsilon_{11}$, reducing the model to the original one-dimensional description [1,22,28].

The free energy density of the mixture is defined by establishing the volume fractions of martensitic variants, β_1 and β_2, which are associated with detwinned martensites ($M+$ and $M-$, respectively) and austenite (A), β_3. The fourth phase is associated with twinned martensite (M) and its volume fraction is β_4.

$$\rho\hat{\Psi}\left(\varepsilon_{ij}, T, \beta_1, \beta_2, \beta_3, \beta_4\right) = \rho\sum_{n=1}^{4}\beta_n\Psi_n(\varepsilon_{ij}, T) + I_\Theta \tag{5}$$

where $I_\Theta = I_\Theta(\beta_1, \beta_2, \beta_3, \beta_4)$is the indicator function associated with the convex set Θ, see Rockafellar [26], that establishes the phase coexistence conditions

$$\Theta = \left\{\beta_n \in \Re, \left| \begin{array}{l} 0 \leq \beta_n \leq 1 \ (n = 1, 2, 3, 4); \quad \sum_{n=1}^{4}\beta_n = 1 \\ \beta_1 = \beta_2 = 0 \quad \text{in stress-free state when} \quad \beta_1^s = \beta_2^s = 0 \end{array}\right.\right\} \tag{6}$$

From these conditions, it is possible to use $\beta_4 = 1 - \beta_1 - \beta_2 - \beta_3$ in order to define a free energy density in terms of only three volume fractions:

$$\rho\Psi(\varepsilon_{ij}, T, \beta_1, \beta_2, \beta_3) = \rho\left[\beta_1(\Psi_1 - \Psi_4) + \beta_2(\Psi_2 - \Psi_4) + \beta_3(\Psi_3 - \Psi_4) + \Psi_4\right] + I_\pi \tag{7}$$

Here, the indicator function $I_\pi = I_\pi(\beta_1, \beta_2, \beta_3)$ is related to the convex set π defined as follows:

$$\pi = \left\{\beta_m \in \Re, \left| \begin{array}{l} 0 \leq \beta_m \leq 1 \ (m = 1, 2, 3); \quad \beta_1 + \beta_2 + \beta_3 \leq 1 \\ \beta_1 = \beta_2 = 0 \quad \text{in stress-free state when } \beta_1^s = \beta_2^s = 0 \end{array}\right.\right\} \tag{8}$$

where β_1^s and β_2^s are the values of β_1 and β_2, respectively, when the phase transformation begins to take place. This is geometrically represented by a tetrahedron in the (β_1, β_2, β_3)-space, shown in Fig. 1.

Therefore, the free energy density of the mixture has the following form:

$$\begin{aligned} \rho\Psi(\varepsilon_{ij}, T, \beta_1, \beta_2, \beta_3) = {} & \alpha(\beta_2 - \beta_1)\Gamma - \Lambda(\beta_1 + \beta_2) + \left(\frac{1}{2}(\lambda^A - \lambda^M)\varepsilon_{kk}^2 + (\mu^A - \mu^M)\varepsilon_{ij}\varepsilon_{ij}\right)\beta_3 \\ & -(\Omega_{ij}^A - \Omega_{ij}^M)(T - T_0)\varepsilon_{ij}\beta_3 - \Lambda_3\beta_3 + \left(\frac{1}{2}\lambda^M\varepsilon_{kk}^2 + \mu^M\varepsilon_{ij}\varepsilon_{ij}\right) \\ & -\Omega_{ij}^M(T - T_0)\varepsilon_{ij} + \Lambda_M + I_\pi \end{aligned} \tag{9}$$

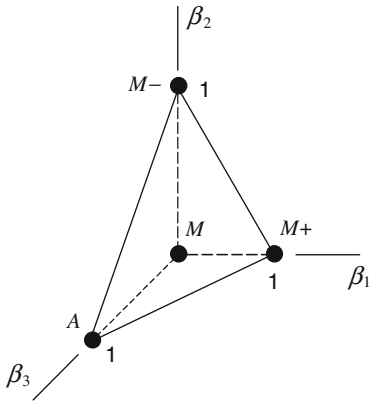

Fig. 1 Tetrahedron of the constraints π

where $\Lambda = 2\Lambda_M$ and $\Lambda_3 = \Lambda_M + \Lambda_A$.

From the generalized standard material approach, the thermodynamical forces associated with each internal variable are defined as follows [12]:

$$\sigma_{ij} = \rho\frac{\partial \Psi}{\partial \varepsilon_{ij}} = \lambda\varepsilon_{kk}\delta_{ij} + 2\mu\varepsilon_{ij} + \alpha\omega_{ij}\,(\beta_2 - \beta_1) - \Omega\delta_{ij}(T - T_0) \tag{10}$$

$$B_1 = -\rho\partial_{\beta_1}\Psi = \alpha\Gamma + \Lambda + \partial_{\beta_1} I_\pi \tag{11}$$

$$B_2 = -\rho\partial_{\beta_2}\Psi = -\alpha\Gamma + \Lambda + \partial_{\beta_2} I_\pi \tag{12}$$

$$\begin{aligned} B_3 = -\rho\partial_{\beta_3}\Psi = &-\left(\frac{1}{2}\lambda^A\varepsilon_{kk}^2 + \mu^A\varepsilon_{ij}\varepsilon_{ij}\right) + \left(\frac{1}{2}\lambda^M\varepsilon_{kk}^2 + \mu^M\varepsilon_{ij}\varepsilon_{ij}\right) + \Lambda_3 \\ &+(\Omega^A - \Omega^M)(T - T_0)\varepsilon_{kk} + \partial_{\beta_3} I_\pi \end{aligned} \tag{13}$$

Here, the $\partial_{\beta_m}(\,)$ represents the subdifferential with respect to β_m. Note that the material parameter is given by a kind of rule of mixtures, being defined as follows:

$$\begin{aligned} \lambda &= \lambda^M + \beta_3(\lambda^A - \lambda^M) \\ \mu &= \mu^M + \beta_3(\mu^A - \mu^M) \\ \Omega_{ij} &= \Omega_{ij}^M + \beta_3(\Omega_{ij}^A - \Omega_{ij}^M) = \Omega\delta_{ij} \end{aligned} \tag{14}$$

It is also important to observe that

$$\omega_{ij} = \frac{1}{3}\delta_{ij} + \left[\frac{3\varepsilon_{ij} - \varepsilon_{kk}\delta_{ij}}{3\sqrt{3}\,|\sqrt{J_2}|}\right]\mathrm{sign}(\varepsilon_{kk}) \tag{15}$$

and that

$$\frac{\partial \mathrm{sign}(\varepsilon_{kk})}{\partial \varepsilon_{ij}} = 0 \tag{16}$$

Moreover, the functions Λ and Λ_3 are temperature dependent:

$$\Lambda = 2\Lambda_M = \begin{cases} -L_0 + \frac{L}{T_M}(T - T_M) & \text{if } T > T_M \\ -L_0 & \text{if } T \le T_M \end{cases} \tag{17}$$

$$\Lambda_3 = \Lambda_M + \Lambda_A = \begin{cases} -L_0^A + \frac{L^A}{T_M}(T - T_M) & \text{if } T > T_M \\ -L_0^A & \text{if } T \le T_M \end{cases} \tag{18}$$

where T_M is the temperature below which the martensitic phase becomes stable. Besides, L_0, L, L_0^A and L^A are parameters related to phase transformation critical stresses. Note that, based on the previous definition, the phase transformation stress level is constant for $T < T_M$.

Since $\lambda\varepsilon_{kk}\delta_{ij} + 2\mu\varepsilon_{ij} = E_{ijkl}\varepsilon_{kl}$, it is possible to rewrite the stress–strain relation as follows:

$$\sigma_{ij} = E_{ijkl}\varepsilon_{kl} + \alpha\omega_{ij}(\beta_2 - \beta_1) - \Omega\delta_{ij}(T - T_0) \tag{19}$$

where $E_{ijkl} = E^M_{ijkl} + \beta_3(E^A_{ijkl} - E^M_{ijkl})$. In case of isotropic materials, Lamé coefficients can be expressed in terms of engineering constants as follows:

$$\lambda = \frac{\upsilon E}{(1+\upsilon)(1-2\upsilon)} \quad \text{and} \quad \mu = G = \frac{E}{2(1+\upsilon)} \tag{20}$$

where E is the elastic modulus, G is the shear modulus and υ is the Poisson ratio.

The thermomechanical behavior of SMAs is intrinsically dissipative, and therefore, it is important to establish the pseudo-potential of dissipation that allows the description of dissipative materials. By assuming that this potential may be split into mechanical and thermal parts, its mechanical part may be considered as follows:

$$\varphi(\dot\beta_1, \dot\beta_2, \dot\beta_3) = \frac{1}{2}(\eta_1\dot\beta_1^2 + \eta_2\dot\beta_2^2 + \eta_3\dot\beta_3^2) + I_x \tag{21}$$

where $I_x = I_x(\dot\beta_1, \dot\beta_2, \dot\beta_3)$ is the indicator function related to the convex set χ, that provides constraints associated with phase transformation evolution. Physically, this indicator function establishes constraints related to internal subloops due to incomplete phase transformations and also to the formation of detwinned martensite (M). Hence, for $\left|\dot\sigma_{ij}\right| = 0$ the convex set χ can be written as follows:

$$\chi = \left\{ \dot\beta_n \in \Re \;\middle|\; \begin{array}{l} \dot T\dot\beta_1 \begin{cases} < 0 & \text{if } \dot T > 0, \quad \sigma_{ij} = 0 \quad \text{and} \quad \beta_1^s \neq 0 \\ = 0 & \text{otherwise} \end{cases} \\ \dot T\dot\beta_2 \begin{cases} < 0 & \text{if } \dot T > 0, \quad \sigma_{ij} = 0 \quad \text{and} \quad \beta_2^s \neq 0 \\ = 0 & \text{otherwise} \end{cases} \\ \dot T\dot\beta_3 \geq 0 \\ -\dot\beta_1^2 - \dot\beta_1\dot\beta_3 = 0 \quad \text{or} \quad -\dot\beta_2^2 - \dot\beta_2\dot\beta_3 = 0 \end{array} \right. \tag{22}$$

Together with constraints related to internal subloops, the set (22) also expresses a constraint to eliminate both $M+ \rightarrow M$ and $M- \rightarrow M$ phase transformations. In mathematical terms, this is expressed by $\dot\beta_1\dot\beta_4 = \dot\beta_1(-\dot\beta_1 - \dot\beta_2 - \dot\beta_3) = -\dot\beta_1^2 - \dot\beta_1\dot\beta_3 = 0$ or by $\dot\beta_2\dot\beta_4 = \dot\beta_2(-\dot\beta_1 - \dot\beta_2 - \dot\beta_3) = -\dot\beta_2^2 - \dot\beta_2\dot\beta_3 = 0$, respectively, which means that when one kind of transformation occurs the other must vanish. Moreover, the discarded terms in both equations $(-\dot\beta_1\dot\beta_2)$ represent impossible transformations and, thus, are not considered. Otherwise, for a system with some kind of mechanical loading $\left|\dot\sigma_{ij}\right| \neq 0$:

$$\chi = \left\{ \dot\beta_n \in \Re \;\middle|\; \begin{array}{lll} \dot\Gamma\dot\beta_1 \geq 0; & \dot\Gamma\dot\beta_3 \leq 0; & \text{if} \quad \Gamma \geq 0 \\ \dot\Gamma\dot\beta_2 \leq 0; & \dot\Gamma\dot\beta_3 \geq 0; & \text{if} \quad \Gamma < 0 \end{array} \right. \tag{23}$$

Under these assumptions, and considering again the generalized standard materials approach, the thermodynamical fluxes are represented as [12]:

$$\partial_{\dot\beta_m}\varphi = \eta_m\dot\beta_m + \partial_{\dot\beta_m} I_\chi = B_m \quad (m = 1, 2, 3), \quad \text{without summation} \tag{24}$$

In order to contemplate different aspects of kinetics of phase transformation, parameter η_i may assume different values for cases of loading or unloading behaviors:

$$\begin{cases} \eta_i = \eta_i^L & \text{if} \quad \dot\Gamma \geq 0 \\ \eta_i = \eta_i^U & \text{if} \quad \dot\Gamma < 0 \end{cases} \tag{25}$$

These equations establish a complete set of constitutive relations, given by:

$$\begin{aligned} \sigma_{ij} &= E_{ijkl}\varepsilon_{kl} + \alpha\omega_{ij}(\beta_2 - \beta_1) - \Omega\delta_{ij}(T - T_0) \\ \dot\beta_1 &= \frac{1}{\eta_1}\left\{\alpha\Gamma + \Lambda + \partial_{\beta_1} I_\pi\right\} - \partial_{\dot\beta_1} I_\chi \\ \dot\beta_2 &= \frac{1}{\eta_2}\left\{-\alpha\Gamma + \Lambda + \partial_{\beta_2} I_\pi\right\} - \partial_{\dot\beta_2} I_\chi \\ \dot\beta_3 &= \frac{1}{\eta_3}\left\{-\frac{1}{2}(\lambda^A - \lambda^M)\varepsilon_{kk}^2 - (\mu^A - \mu^M)\varepsilon_{ij}\varepsilon_{ij} + \Lambda_3 + (\Omega^A - \Omega^M)(T - T_0)\varepsilon_{kk} + \partial_{\beta_3} I_\pi\right\} - \partial_{\dot\beta_3} I_\chi \end{aligned} \tag{26}$$

Table 1 Model parameters

E_A (GPa)	E_M (GPa)	α (MPa)	Ω_A (MPa/K)	Ω_M (MPa/K)
54	42	330	0.74	0.17
L_0 (MPa)	L (MPa)	L_0^A (MPa)	L_A (MPa)	T_M (K)
0.15	41.5	0.63	185	291.4
T_A (K)	η^L (MPa s)	η^U (MPa s)	η_3^L (MPa s)	η_3^U (MPa s)
307.5	1	2.7	1	2.7
	ν^A	ν^M		
	0.2	0.35		

Nonlinearities of the formulation are treated by considering an iterative numerical procedure based on the operator split technique [19]. The procedure is similar to that employed earlier for the one-dimensional media, see [28] and [22]. The procedure isolates the subdifferentials and uses the implicit Euler method combined with an orthogonal projection algorithm to evaluate evolution equations. Orthogonal projections assure that volume fractions obey the imposed constraints. In order to satisfy constraints expressed in Eq. (9), values of volume fractions must stay inside or on the boundary of π, the tetrahedron shown in Fig. 1.

In order to evaluate the capability of the above introduced model to describe thermomechanical behavior of SMAs, numerical results from the uniaxial and multiaxial single-point tests are carried out. Specifically, uniaxial tests show pseudoelasticity, shape memory effect, phase transformation due to temperature variations and internal subloops due to incomplete phase transformations. Concerning multiaxial tests, the pure shear stress and hydrostatic tests are discussed showing qualitatively coherent results. Moreover, other tensile–shear tests are conducted modeling the general three-dimensional behavior of SMAs. Table 1 presents model parameters employed for all numerical simulations.

3 Numerical simulations: uniaxial tests

In order to evaluate the capability of the proposed model to describe thermomechanical behavior of SMAs, let us consider uniaxial tests related to a single-point tensile behavior, assuming that $\Gamma = \varepsilon_{11}$ and $\nu = 0$. Initially, let us consider a pseudoelastic tensile test by treating different, constant temperatures. The mechanical loading is linearly applied from a stress-free state, passing through a maximum value, and then linearly returning back to a stress-free state. The maximum stress tensor has the following form:

$$\sigma_{ij}^T = \begin{bmatrix} 5 & 0 & 0 \\ 0 & 0 & 0 \\ 0 & 0 & 0 \end{bmatrix} \text{GPa}$$

Under this condition, there is a stress-induced phase transformation from austenite to detwinned martensite $M+$, and the increase in the temperature changes the hysteresis loop position. The model is capturing the expected pseudoelastic effect and its temperature dependence (see Fig. 2).

The proposed model is capable of describing internal subloops due to the incomplete phase transformations. A pseudoelastic response is considered by imposing a mechanical loading process shown in Fig. 3, together with a fixed constant temperature. This loading process induces incomplete phase transformations, as can be observed in Fig. 3. This is an important characteristics related to SMA response, which is captured by the proposed model. Figure 3 also shows the volume fraction evolution of the phases.

Let us now focus our attention on the shape memory effect. The SMA specimen starts at $T = 260$ K, a temperature where martensite is stable, and then is subjected to a mechanical loading. After the loading–unloading process, the specimen is subjected to a temperature change. Figure 4 presents the thermomechanical loading process. At the beginning of the process, the mechanical loading is applied at a low temperature, upon final unloading there is still some residual strain, which can be fully recovered by heating the sample until austenite becomes stable and cooling back to the test temperature. Figure 4 presents stress–strain–temperature curve showing the complete process and the corresponding volume fraction evolution. Initially, the mechanical loading causes the reorientation from M to $M+$. Afterward, the temperature change causes the phase transformation from $M+$ to A, which is responsible for residual strain recovery.

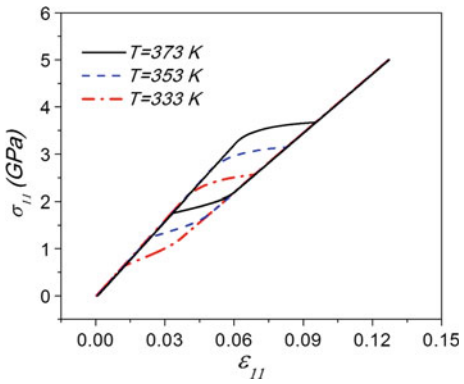

Fig. 2 Pseudoelastic behavior for different temperatures

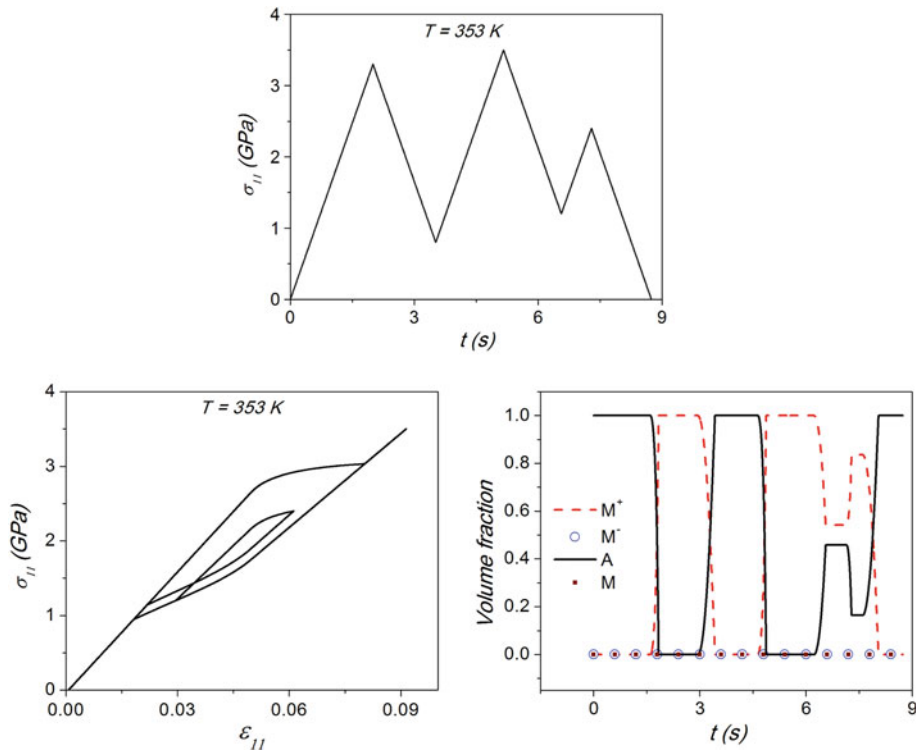

Fig. 3 Internal subloops due to the incomplete phase transformations

Let us now consider the phase transformations induced by temperature variations in a stress-free state. The temperature is linearly increased from $T = 230\,\mathrm{K}$ to $T = 333\,\mathrm{K}$ and then linearly decreased back to $T = 230\,\mathrm{K}$. Figure 5 presents the strain–temperature curve together with volume fraction evolution. It is noticeable that the SMA specimen presents a phase transformation from M to A and then the reverse transformation, presenting a hysteresis loop.

4 Numerical simulations: multiaxial tests

This section deals with multiaxial tests that are used to show the capabilities of the above introduced three-dimensional model. Initially, pure shear and hydrostatic tests are performed in order to verify the consistence of the model. Afterward, some other tests are carried out in order to compare our results with the published

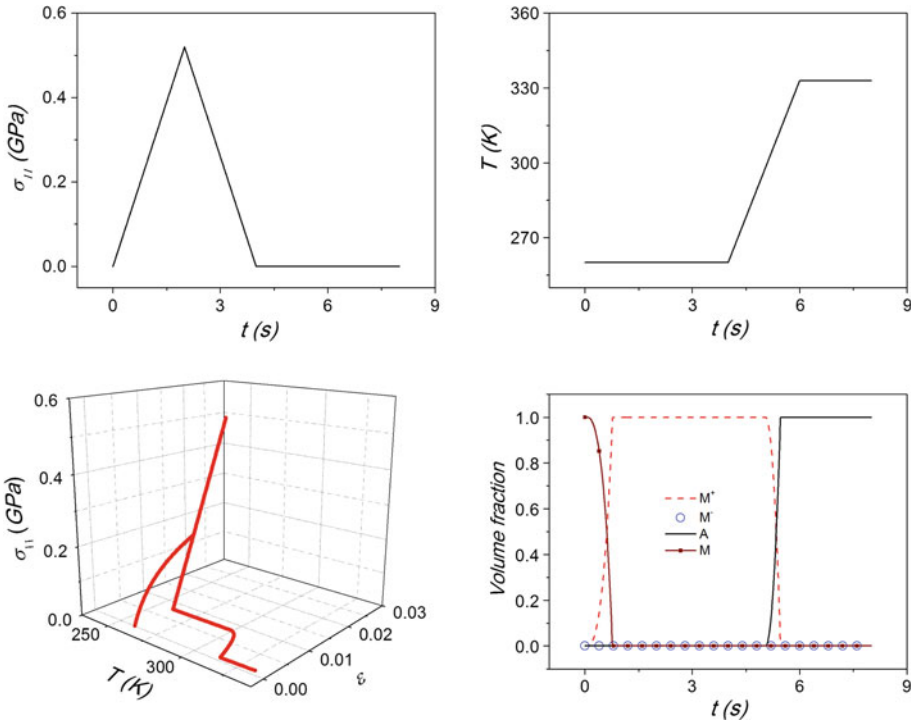

Fig. 4 Shape memory effect

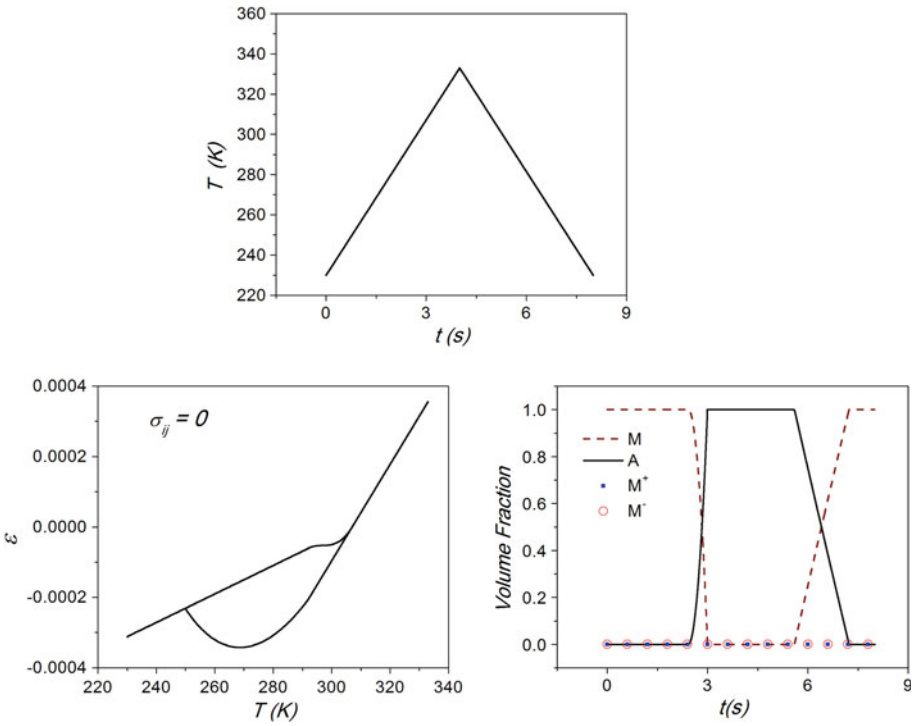

Fig. 5 Phase transformation due to the temperature variation

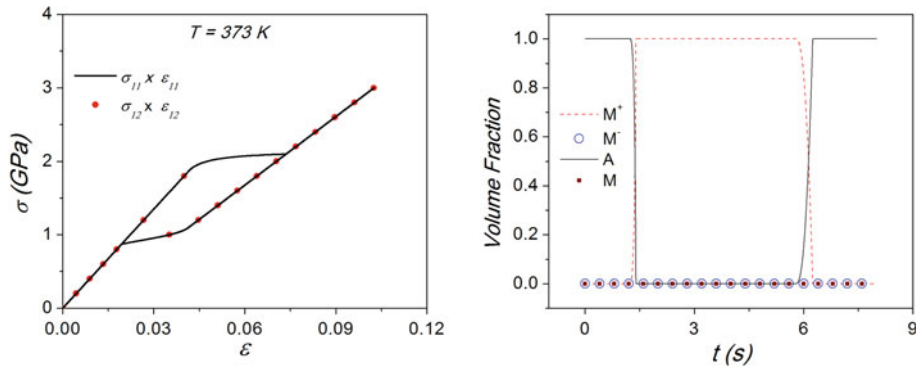

Fig. 6 Pure shear test

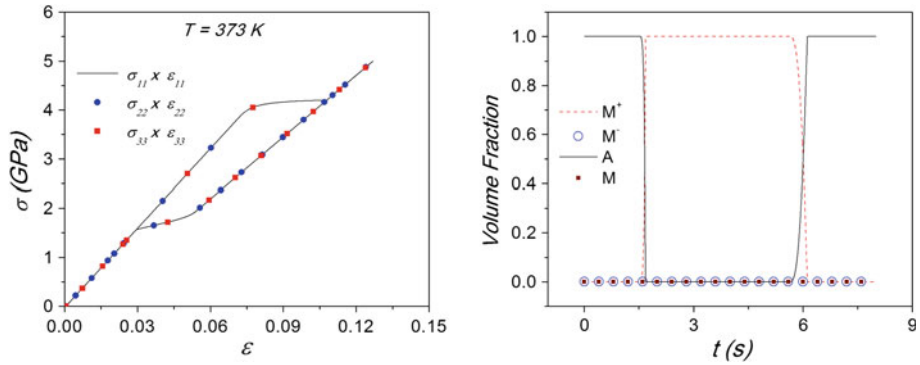

Fig. 7 Hydrostatic test

data. Namely, the tensile–shear test is conducted where the loading is applied independently [23,27] and a coupled tensile–shear test is carried out [33].

4.1 Pure shear test

The analysis of a pure shear stress test allows us to verify the coordinate invariance by establishing a comparison between the pure shear state with the one with tensile and compressive stress of the same value. Therefore, the maximum values of the stress tensors of these two states are given by:

$$\sigma_{ij}^{A} = \begin{bmatrix} 3 & 0 & 0 \\ 0 & -3 & 0 \\ 0 & 0 & 0 \end{bmatrix} \text{GPa} \quad \sigma_{ij}^{B} = \begin{bmatrix} 0 & 3 & 0 \\ 3 & 0 & 0 \\ 0 & 0 & 0 \end{bmatrix} \text{GPa}$$

Tests are carried out at temperature $T = 373$ K, which coincides with the temperature T_0. Figure 6 shows the SMA response presenting the stress–strain curves and the volume fraction evolution, comparing the following curves: $\sigma_{11} \times \varepsilon_{11}$ and $\sigma_{12} \times \varepsilon_{12}$. The response is a typical pseudoelastic behavior and it is important to note that curves are identical, confirming the system invariance.

4.2 Hydrostatic test

Let us now consider a hydrostatic test imposing a loading process with the maximum stress tensor

$$\sigma_{ij}^{H} = \begin{bmatrix} 5 & 0 & 0 \\ 0 & 5 & 0 \\ 0 & 0 & 5 \end{bmatrix} \text{GPa}$$

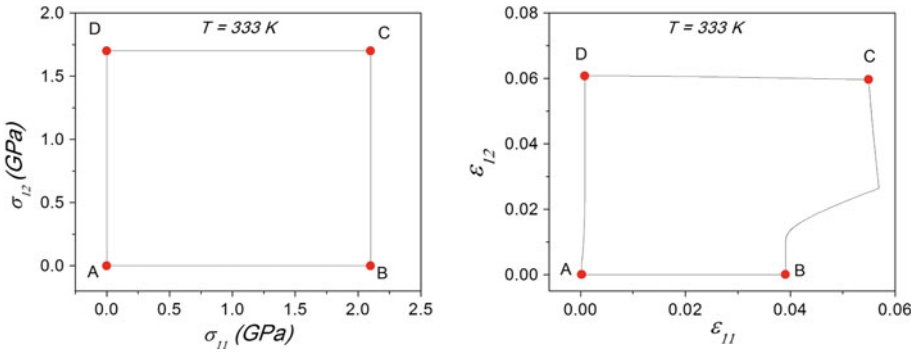

Fig. 8 Tensile–shear test

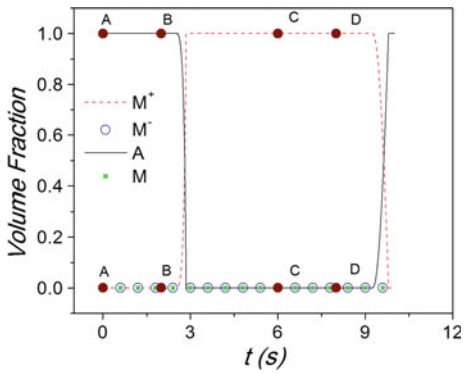

Fig. 9 Tensile–shear test: volume fraction evolutions

Once again, the test is performed at temperature $T = 373$ K and, as expected, the SMA presents similar pseudo-elastic behavior in the three directions. Figure 7 presents the stress–strain curves together with volume fraction evolution.

4.3 Tensile–shear test

A tensile–shear test is now carried out, and results by [23] that uses the experimental tests of [27], are used as reference. The loading process is shown in Fig. 8 (left side), representing a situation where a tensile loading is applied with a linear increase until a maximum value of 2.1 GPa is reached. Afterward, a shear stress is applied with a linear increase until the value of 1.7 GPa is reached, keeping the tensile load constant. Then, similar procedure is adopted in order to remove both loads. Figure 8 (right side) presents the strain space resulting from this loading process. The nonlinearity of the curve is clearly noticeable. Since the shear loading is applied keeping the tensile load constant, great part of the phase transformation is induced when shear load is applied, see Fig. 9 that presents the volume fraction evolution. It is also important to observe that the positive volume fraction is induced as a consequence of the inductor characteristics ($\Gamma \geq 0$).

Figure 10 shows the stress–strain curves presenting the nonlinear aspects of the stress–strain curves. These results have a qualitative agreement with tests performed by [23] showing the capability of the above introduced model to describe this kind of three-dimensional behavior.

4.4 Coupled tensile–shear test

A tensile–shear test is now carried out by considering a coupled loading process, which means that both loadings are applied together. This analysis is inspired on the tension/torsion-internal pressure tests conducted by [33], which reproduces the behavior of a cylindrical NiTi tube. Here, an SMA specimen is subjected to a loading history presented in Fig. 11 at temperature $T = 373$ K. It is representing a situation where the axial pressure increases with the increase of the torsional angles. Once the axial loading starts, the shear stresses

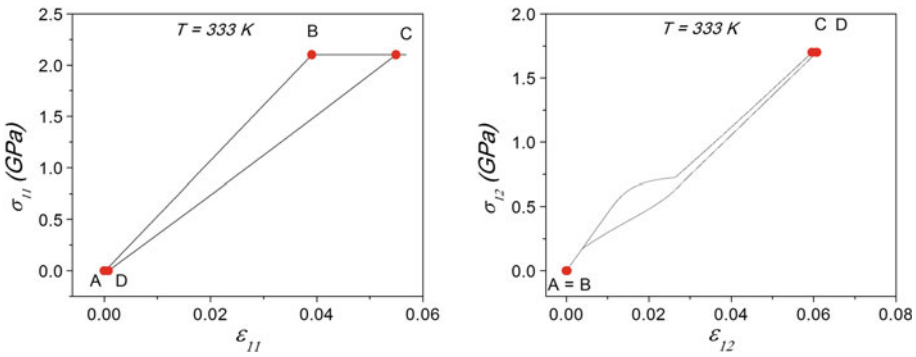

Fig. 10 Tensile–shear test: stress–strain curves

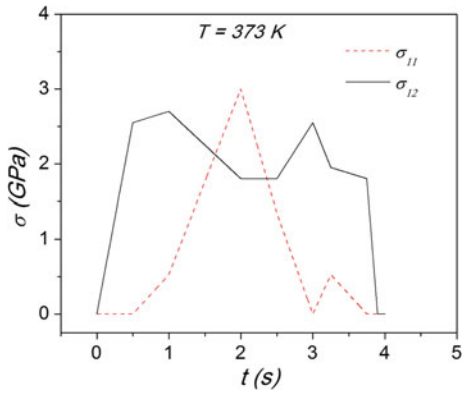

Fig. 11 Coupled tensile–shear test: loading

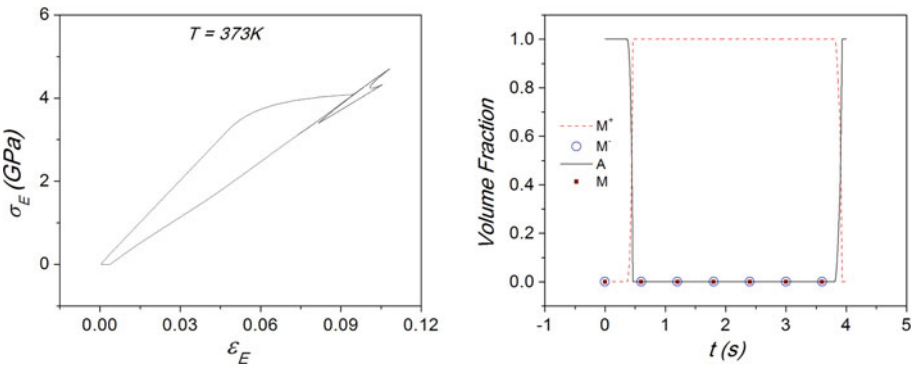

Fig. 12 Coupled tensile–shear test: equivalent stress–strain curve

decrease rapidly then decrease gradually with the increasing of the axial stresses at applied constant torsional angles. Under these conditions, the tensile stress reaches its maximum when the shear stress achieves the minimum.

Wang et al. [33] evaluate the multiaxial thermomechanical behavior of SMAs by considering equivalent stress and strain defined as follows:

$$\sigma_E = \sqrt{(\sigma_{11})^2 + 3(\sigma_{12})^2} \tag{27}$$

$$\varepsilon_E = \sqrt{(\varepsilon_{11})^2 + \frac{4}{3}(\varepsilon_{12})^2} \tag{28}$$

Equivalent stress–strain curve of this tensile–shear test is shown in Fig. 11. The general behavior presents an austenite-martensite phase transformation followed by the reverse transformation. The hysteresis is char-

acterized by an irregular behavior in the equivalent stress–strain space, as observed in Fig. 12. This result is qualitatively consistent with data presented in [33].

5 Conclusions

The present work proposes a novel three-dimensional constitutive model to describe the thermomechanical behavior of shape memory alloys. The phenomenological model is developed within the framework of continuum mechanics and the generalized standard materials. Inspired on one-dimensional models, four macroscopic phases are considered assuming different properties for austenitic and martensitic phases. Martensitic reorientation is defined by an equivalent field that includes either the volumetric expansion or the deviatoric effect. Numerical simulations are carried out for uniaxial and multiaxial single-point tests. Uniaxial tests represent the typical thermomechanical behavior of tensile tests showing pseudoelasticity, shape memory effect, phase transformation due to the temperature variations and internal subloops due to the incomplete phase transformations. Multiaxial tests are carried out in order to evaluate the capabilities of the introduced model to describe different thermomechanical loadings. Pure shear and hydrostatic cases are explored showing a qualitative coherence and presenting important characteristics of the model as the coordinate invariance. Finally, some tensile–shear tests are performed. Initially, the uncoupled loading is considered. Afterward, a coupled loading is conducted. Both cases present results that are in qualitative agreement with the related data reported in the literature. Therefore, it is possible to conclude that the proposed three-dimensional model captures the general thermomechanical behavior of SMAs in both uniaxial and multiaxial tests presenting qualitative coherent results.

Acknowledgments The authors would like to acknowledge the support of the Brazilian Research Agencies CNPq and FAPERJ and through the INCT-EIE (National Institute of Science and Technology—Smart Structures in Engineering) the CNPq and FAPEMIG. The Natural Sciences and Engineering Research Council of Canada (NSERC) and the Air Force Office of Scientific Research (AFOSR) is also acknowledged.

References

1. Aguiar, R.A.A., Savi, M.A., Pacheco, P.M.C.L.: Experimental and numerical investigations of shape memory alloy helical springs. Smart Mater. Struct. (2010). doi:10.1088/0964-1726/19/2/025008
2. Auricchio, F., Reali, A., Stefanelli, U.: A three-dimensional model describing stress-induced solid phase transformation with permanent inelasticity. Int. J. Plast. **23**, 207–226 (2007)
3. Baêta-Neves, A.P., Savi, M.A., Pacheco, P.M.C.L.: On the Fremond's constitutive model for shape memory alloys. Mech. Res. Commun. **31**(6), 677–688 (2004)
4. Brocca, M., Brinson, L.C., Bazant, Z.P.: Three-dimensional constitutive model for shape memory alloys based on microplane model. J. Mech. Phys. Solids **50**, 1051–1077 (2002)
5. Fremond, M.: Shape memory alloy: a thermomechanical macroscopic theory. CISM Courses and Lectures, 351, New York (1996)
6. Gall, K., Sehitoglu, H.: The role of texture in tension-compression asymmetry in polycrystalline Ni–Ti. Int. J. Plast. **15**, 69–92 (1999)
7. Grabe, C., Bruhns, O.T.: Tension/torsion tests of pseudoelastic, polycrystalline NiTi shape memory alloys under temperature control. Mater. Sci. Eng. A (2007). doi:10.101111111116/j.msea.2007.03.117
8. Jackson, C.M., Wagner, H.J., Wasilewski, R.J.: 55-Nitinol—the alloy with a memory: its physical metallurgy, properties, and applications. NASA-SP-5110 (1972)
9. Kalamkarov, A.L., Kolpakov, A.G.: Analysis, Design and Optimization of Composite Structures. Wiley, Chichester (1997)
10. Lagoudas, D.C.: Shape Memory Alloys: Modeling and Engineering Applications. Springer, New York (2008)
11. Lagoudas, D.C., Entchev, P.B., Popov, P., Patoor, E., Brinson, L.C., Gao, X.: Shape memory alloys, part II: modeling of polycrystals. Mech. Mater. **38**, 430–462 (2006)
12. Lemaitre, J., Chaboche, J.L.: Mechanics of Solid Materials. Cambridge University Press, Cambridge (1990)
13. Levitas, V.I., Preston, D.L., Lee, D.-W.: Three-dimensional Landau theory for multivariant stress-induced martensitic phase transformations III. Alternative potentials, critical nuclei, kink solutions, and dislocation theory. Phys. Rev. B **68**, 134201 (2003)
14. Machado, L.G., Savi, M.A.: Medical applications of shape memory alloys. Braz. J. Med. Biol. Res. **36**(6), 683–691 (2003)
15. Manach, P., Favier, D.: Shear and tensile thermomechanical behavior of near equiatomic NiTi alloy. Mater. Sci. Eng. A **222**, 45–47 (1997)
16. Matsumoto, O., Miyazaki, S., Otsuka, K., Tamura, H.: Crystallography of martensitic-transformation in Ti–Ni single crystals. ACTA Metall. **35**(8), 2137–2144 (1987)
17. McNaney, J.M., Imbeni, V., Jung, Y., Papadopoulos, P., Ritchie, R.O.: An experimental study of the superelastic effect in a shape-memory Nitinol alloy under biaxial loading. Mech. Mater. **35**, 969–986 (2007)

18. Monteiro, P.C.C. Jr., Savi, M.A., Netto, T.A., Pacheco, P.M.C.L.: A phenomenological description of the thermomechanical coupling and the rate-dependent behavior of shape memory alloys. J. Intell. Mater. Syst. Struct. **20**(14), 1675–1687 (2009)
19. Ortiz, M., Pinsky, P.M., Taylor, R.L.: Operator split methods for the numerical solution of the elastoplastic dynamic problem. Comput. Methods Appl. Mech. Eng. **39**, 137–157 (1983)
20. Otsuka, K., Ren, X.: Recent developments in the research of shape memory alloys. Intermetallics **7**, 511–528 (1999)
21. Paiva, A., Savi, M.A.: An overview of constitutive models for shape memory alloys. Math. Probl. Eng. Article ID 56876, 1–30 (2006)
22. Paiva, A., Savi, M.A., Braga, A.M.B., Pacheco, P.M.C.L.: A constitutive model for shape memory alloys considering tensile-compressive asymmetry and plasticity. Int. J. Solids Struct. **42**(11–12), 3439–3457 (2005)
23. Panico, M., Brinson, L.C.: A three-dimensional phenomenological model for martensite reorientation in shape memory alloys. J. Mech. Phys. Solids **55**(11), 2491–2511 (2007)
24. Patoor, E., Lagoudas, D.C., Entchev, P.B., Brinson, L.C., Gao, X.: Shape memory alloys, part I: general properties and modeling of single crystals. Mech. Mater. **38**, 391–429 (2006)
25. Popov, P., Lagoudas, D.C.: A 3-D constitutive model for shape memory alloys incorporating pseudoelasticity and detwinning of self-accommodated martensite. Int. J. Plast. **23**, 1679–1720 (2007)
26. Rockafellar, R.T.: Convex Analysis. Princeton Press, Princeton, New Jersey (1970)
27. Sittner, P., Hara, Y., Tokuda, M.: Experimental-study on the thermoelastic martensitic-transformation in shape-memory alloy polycrystal induced by combined external forces. Metall. Mater. Trans. A Phys. Metall. Mater. Sci. **26**(11), 2923–2935 (1995)
28. Savi, M.A., Paiva, A., Baêta-Neves, A.P., Pacheco, P.M.C.L.: Phenomenological modeling and numerical simulation of shape memory alloys: a thermo-plastic-phase transformation coupled model. J. Intell. Mater. Syst. Struct. **13**(5), 261–273 (2002)
29. Savi, M.A., Paiva, A.: Describing internal subloops due to incomplete phase transformations in shape memory alloys. Arch. Appl. Mech. **74**(9), 637–647 (2005)
30. Schroeder, T.A., Wayman, C.M.: The formation of martensite and the mechanism of the shape memory effect in single crystals of Cu–Zn alloys. ACTA Metall. **25**, 1375 (1977)
31. Shaw, J.A., Kyriades, S.: Thermomechanical aspects of Ni–Ti. J. Mech. Phys. Solids **43**(8), 1243–1281 (1995)
32. Souza, A.C., Mamiya, E., Zouain, N.: Three-dimensional model for solids undergoing stress-induced phase transformations. Eur. J. Mech. A Solids **17**, 789–806 (1998)
33. Wang, Y.F., Yue, Z.F., Wang, J.: Experimental and numerical study of the superelastic behaviour on NiTi thin-walled tube under biaxial loading. Comput. Mater. Sci. **40**(2), 246–254 (2007)
34. Zaki, W., Moumni, Z.: A three-dimensional model of the thermomechanical behavior of shape memory alloys. J. Mech. Phys. Solids (2007). doi:10.1016/j.jmps.2007.03.012
35. Zhang, X.D., Rogers, C.A., Liang, C.: Modeling of two-way shape memory effect. Smart Struct. Mater. ASME, pp. 79–90 (1991)